NANO · MICRO small
www.small-journal.com

Ultrahigh-Energy Density Lithium-Ion Cable Battery Based on the Carbon-Nanotube Woven Macrofilms

Ziping Wu, Kaixi Liu, Chao Lv, Shengwen Zhong, Qinghui Wang, Ting Liu, Xianbin Liu, Yanhong Yin, Yingyan Hu, Di Wei,* and Zhongfan Liu**

Moore's law predicts the performance of integrated circuit doubles every two years, lasting for more than five decades. However, the improvements of the performance of energy density in batteries lag far behind that. In addition, the poor flexibility, insufficient-energy density, and complexity of incorporation into wearable electronics remain considerable challenges for current battery technology. Herein, a lithium-ion cable battery is invented, which is insensitive to deformation due to its use of carbon nanotube (CNT) woven macrofilms as the charge collectors. An ultrahigh-tap density of 10 mg cm^{-2} of the electrodes can be obtained, which leads to an extremely high-energy density of 215 mWh cm^{-3}. The value is approximately seven times than that of the highest performance reported previously. In addition, the battery displays very stable rate performance and lower internal resistance than conventional lithium-ion batteries using metal charge collectors. Moreover, it demonstrates excellent convenience for connecting electronics as a new strategy is applied, in which both electrodes can be integrated into one end by a CNT macrorope. Such an ultrahigh-energy density lithium-ion cable battery provides a feasible way to power wearable electronics with commercial viability.

Energy storage devices present a significant challenge in developing a robust deformable system to seamlessly integrate with intelligent wearable electronics.[1–3] Lithium-ion batteries (LIBs) are considered promising power sources for deformable functions if they can be stretched, compressed, rolled, deformed, and even folded.[4–7] To this end, several recent studies have tried to realize flexible and even foldable batteries with a 2D planar structure.[8–15] Comparing such 2D planar structure with conventional 3D bulky structure, unique 1D cable structure allows LIBs to be deformable in all dimensions, and its size can also be lessened and woven into textiles to satisfy different shapes for human bodies.[16,17]

To realize the concept, LG Chem. Ltd. first achieved cable-shaped flexible LIBs based on hollow multihelix electrodes in 2012.[18] Subsequently, several types of batteries with the cable shape have been developed by Peng and other groups.[19–33] For example, the cable battery electrode could be obtained after the metallic current collectors were immersed[20,21] or electrochemically deposited[22] into active material suspension or that sputtered on current collectors, followed by twisting treatment.[23–25] Lithium-sulfur batteries[26–28] and sodium-ion batteries[29] with cable shape have also been demonstrated through a similar method. Zinc air,[30,31] aluminum air,[32] and lithium air[33,34] with 1D structure have been achieved through loading electrocatalysts on the electrode as well. Different cable-shaped batteries displayed different specific capacities and flexibilities. Limited to current technologies, tap densities of active materials on present flexible and thin current collectors are not high, resulting in low-energy densities. In addition, both the gravimetric and volumetric energy density will be reduced further if metals such as Cu or Al are used as charge collectors due to the increase in both weight and volume of packages. Moreover, the metals used in batteries are not suitable when worn on the body. In addition to the above problems, the present structures of the reported cable-shaped batteries are not always convenient to be connected to electronics because the positive and negative tabs are generally placed at each end of the cable to avoid short circuit.

In this study, we report an ultrahigh-energy density lithium-ion cable battery based on carbon nanotube (CNT) woven macrofilms (CMFs). Free-standing CMFs are used to load active materials with ultrahigh-tap density. Flexible CNT macrorope (CMR) is integrated in the center to connect one tab, leading both tabs in one end of the cable battery for excellent convenience to connect electronics. Compared with previous studies, the stable performance of our battery is insensitive to

Dr. Z. Wu, K. Liu, C. Lv, Prof. S. Zhong, Q. Wang, T. Liu, Dr. X. Liu, Dr. Y. Yin, Y. Hu
School of Materials Science and Engineering
Jiangxi University of Science and Technology
86 Hong Qi Road, Ganzhou 341000, P. R. China
E-mail: wuziping724@jxust.edu.cn
Dr. Z. Wu, Prof. Z. Liu
Center for Nanochemistry (CNC)
College of Chemistry and Molecular Engineering
Peking University
Beijing 100871, P. R. China
E-mail: zfliu@pku.edu.cn
Dr. D. Wei, Prof. Z. Liu
Beijing Graphene Institute
Beijing 100094, P. R. China
E-mail: weidi-cnc@pku.edu.cn
The ORCID identification number(s) for the author(s) of this article can be found under https://doi.org/10.1002/smll.201800414.

DOI: 10.1002/smll.201800414

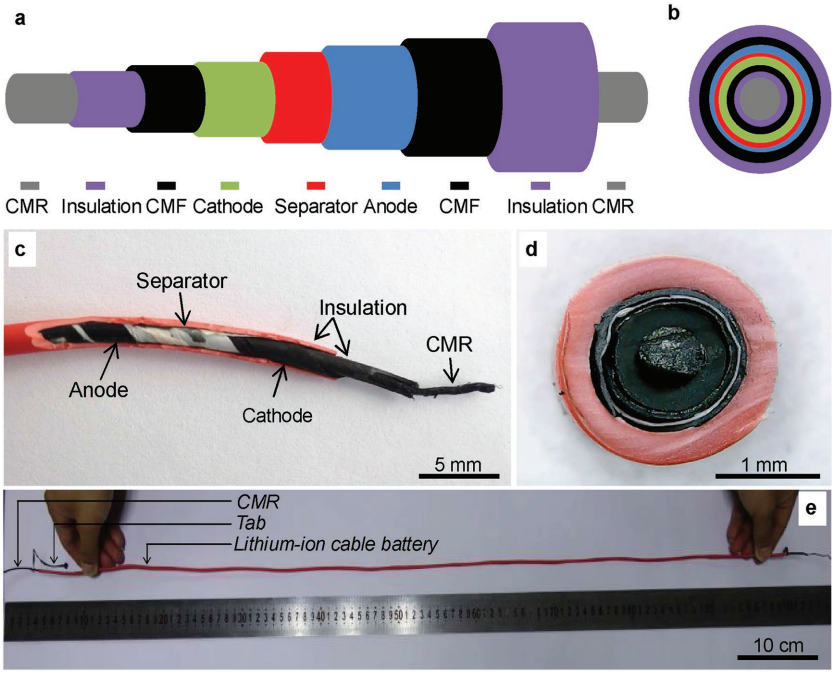

Figure 1. Schematic diagram and prototype of the lithium-ion cable battery. a) Side view; b) cross-section; c) the side-view photograph of the lithium-ion cable battery; d) cross-section; and e) the prototype of lithium-ion cable battery including CMR.

deformation and it could be bent down to less than 4 mm. Importantly, the active materials were infiltrated into the porous surface of the CMF, which mitigates delamination. Thus, active materials with high-tap density are strongly adhered to CMF, increasing the tap density to 10 mg cm^{-2}, leading to extremely high-energy density of 215 mWh cm^{-3}.[8–15,19–34] This value is approximately seven times than that of the highest performance as previously reported. The lithium-ion cable battery reported in this study displays full flexibility, convenient weaving, high-energy density, and scalability of manufacturing, showing applications in wearable electronics with commercial viability.

Figure 1 is a schematic and photograph of the lithium-ion cable battery. As illustrated in Figure 1a,b, the design comprises the CMR, insulation layer, cathode, separator, anode, and the electrolyte. Flexible electrodes and separator were wrapped around the cable-shaped structure layer by layer, which is shown in Figure S1 (Supporting Information). To avoid contact between the CMF and CMR, the insulation layer between them was used. The electrodes with ultrahigh-tap densities and other components are tightly attached to each other, resulting in a flexible lithium-ion cable battery that can be stretched, compressed, rolled, or deformed. Generally, the diameter of the cable-shaped battery is about several millimeters, which makes the positive and negative tabs quite near to each other. If the two tabs are arranged at the same end, they are easily contacted and short circuit occurs. The CMR in the center of the battery strengthened the mechanical property of the assembled cable. Furthermore, the CMR in the core serves as a flexible conductivity, and the positive and negative tabs in each end of the cable battery could be integrated at the same side, thereby leading to convenient processing technology, for example, the obtained lithium-ion cable battery can be integrated into the weaving or knitting process. The side view and cross-sectional structure of the battery was observed by cutting the cable. The optical images (Figure 1c,d) show the well-constructed morphology of the cable, including CMR, inner insulation layer, cathode, separator, anode, and outer insulation layer. The tight combination of the different flexible parts in the LIB is displayed clearly, which may lead to stable electrochemical performances and excellent flexibility. We prepared a prototype of the lithium-ion cable battery, as shown in Figure 1e. The flexible cable has a length of 1200 mm with a diameter of about 2 mm.

Figure 2 shows the morphology of CMR and performance of CMF current collector before and after the active material was coated. The prepared CMR with several meters is lightweight, flexible, and can be stretched, bent, or folded easily as shown in Figure 2a. It can also be twisted or undone easily without any interfiber adhesion, thus indicating high strength and flexibility. The good electrical conductivity of the CMR has been demonstrated in detail in our previous studies.[35] The as-prepared CMFs at 2800 mm length and 50 mm width are very lightweight (less than 1 g) as illustrated in Figure 2b. In addition, the CMF can also be bent, folded, or tailored easily, exhibiting no destructive changes for themselves. Thereby, CMFs indicate a good structure uniformity and flexibility. The strength of the CMF has also been demonstrated in Movie S1 (Supporting Information). Therefore, different active materials could be loaded on them. The surface of the CMF is porous and consists of entangled nanotube bundles that form an interconnected network (as shown in Figure S2a of the Supporting Information). The active materials of $LiCoO_2$ (LCO) and $Li_4Ti_5O_{12}$ (LTO) can be observed in the X-ray diffraction (XRD) patterns, as shown in Figure S2b,c (Supporting Information). After the active material slurries were coated on CMF and then dried, it is intact on the CMF as shown in Figure 2c (and Figure S3a, Supporting Information). Moreover, the tap density of the anode active materials on the CMF increased to a remarkably high mass loading of 10 mg cm^{-2}. The results showed that the active materials coated on CMF are flat and show good durability making the formed electrode display excellent mechanical flexibility. When the electrode was rolled up, the active materials remain intact on CMF, without any anode or cathode active materials detached from the current collectors, as shown in Figure S3b (Supporting Information). From the typical images of Figure S3c,d (Supporting Information), it can be seen clearly that LCO has been infiltrated into CMF, in contrast to the LCO-metallic film where there is a space between active materials and metallic foil. The results demonstrated strong interfacial bonding between the active materials and the CMF. As a parallel experiment, both the CMF and commercial Cu foil loaded with the same amount of anode material have been folded in half. The results are shown in Figure 2d–g. In the case

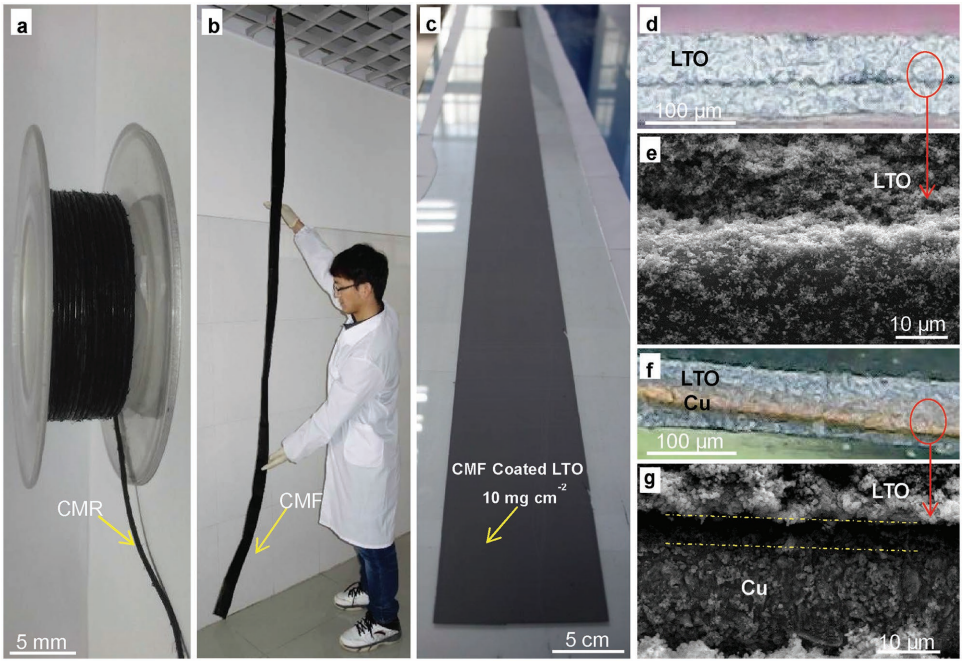

Figure 2. The morphology of CMR, CMF, and after active material coated. a) The photograph of CMR and b) CMF; c) LTO with ultrahigh-tap density coated on the CMF; d) optical microscopy and e) SEM image of the LTO-CMF electrode without cracks after being folded in half; and f) optical microscopy and g) SEM image of LTO-Cu-formed cracks after being folded.

of LTO-CMF electrode, the LTO remains intact on the CMF, although a slight line can be observed in Figure 2d. The scanning electronic microscopy (SEM) image shown in Figure 2e indicated that the LTOs are still connected together despite the fact that the slight line occurred. In contrast, the covered Cu foil was clearly revealed after it has been folded, showing a large space between LTO and Cu foil (Figure 2f,g). The results indicate that some of the LTO layers have been completely detached from the LTO-Cu electrode. This result may be attributed to the porous surface of the CMFs, enabling active material to infiltrate into and integrate with the CMF structure. The roughened surfaces and nanoporous architectures could improve the interface of the current collector and active material.[36–38] On the other hand, electrode slurries cannot penetrate deeply into the surface of any commercial metal current collectors, and thus, their durability is poor when subjected to deformation cycles in flexible or foldable devices. The CMRs, CMFs, and CMF-based electrodes are mass produced with excellent flexibility, good electrical conductivity, and stable performance, indicating the viability for commercial applications.

Stable electrochemical performances of the flexible lithium-ion cable battery could be obtained because of the strong interfacial bonding between the active material and CMF interface. The rate performance and other electrochemical behavior of the lithium-ion cable battery are evaluated in **Figure 3**. In general, the rate performance of a battery can be reflected by capacity maintenance at different rates. To explore the effect of charge/discharge rate (C-rate) on the performance, the lithium-ion cable battery was discharged at different C-rates from 0.1 to 3 C (1 C of current density is ≈0.15 A g^{-1}) and then discharged again at 0.1 C. Note that a C-rate of nC means that battery charges/discharges in $1/n$ hour. The charge or discharge processes of the lithium-ion cable battery exhibit similar trends of performance shown in Figure 3a, and the specific capacity retention of both processes is about 100% at 0.1–1 C. The difference in the performance of the two processes magnifies as C-rate increases. However, the variation in the capacity (C/C_0) does not exceed 5% at 3 C and is quite negligible at low C-rates (inset in Figure 3a). C and C_0 correspond to the specific capacities of different cycles and of the first cycle. These results indicate that our flexible battery could serve as a viable replacement for conventional battery at C-rates of 0.1–1 C, which is the typical range for flexible electronics. Galvanostatic discharge profiles at different cycles of the flexible cable at 0.5 and 1 C can also be seen in Figure S4 (Supporting Information). The lithium-ion cable battery exhibits a high-insertion capacity of 135 mAh g^{-1}. The deinsertion capacity is ≈114–131 mAh g^{-1} at 0.5 and 1 C. Therefore, the majority of Li^+ can be intercalated in electrodes and can also be deintercalated from electrodes. The stability of the battery at operation state is demonstrated in Figure 3b,c. The open-circuit voltage of the full flexible cable is always ≈2.6 V whether it maintains releasing or wrapped state. In addition, similar charge/discharge curves and electrochemical impedance spectroscopy (EIS) of the battery at releasing or different wrapped number can also be seen in Figure S4c,d (Supporting Information). Movie S2 (Supporting Information) also demonstrates such stable properties. To demonstrate the excellent flexibility and cycle performance when the cable battery is bent or twisted, it was tested in the releasing state during the first 30 cycles and then in twisting state for another 40 cycles. In the remaining 30 cycles, the battery was untwisted and tested in releasing state. The specific capacity of the cable-shaped battery is quite insensitive to state of deformation if the C-rate was ≈0.5 C as shown in Figure 3c. If the C-rate increased to ≈1 C, the

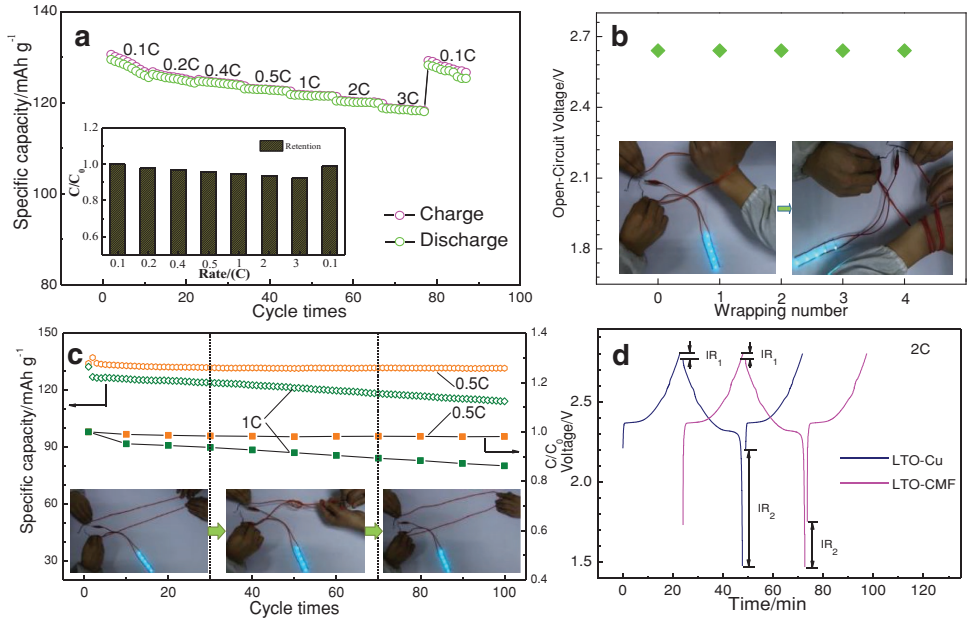

Figure 3. The electrochemical performance of the lithium-ion cable battery. a) Rate performance of the cable and the inset shows the dependence of specific capacity on current rate; b) the dependence of the open-circuit voltage on wrapping number of the battery, correlation of C and C_0 to the specific capacities of different cycle and the first cycle; c) cycling performance and the dependence of specific capacity on the number of cycle times of the device between releasing and twisting states; and d) galvanostatic charge/discharge of the LTO-CMF and LTO-Cu electrodes at charge/discharge rates of ≈2 C.

capacity retention of the battery will be decreased to 86.2%. The coulombic efficiency during the entire releasing and twisting process was nearly 100%. These results demonstrate that performance of the battery is largely unaffected by the deformation process. In addition, similar performance of the battery can be observed after being twisted 100 cycles (Figure S5a, Supporting Information), or at releasing and twisting states after more than 100 twisting cycles. The battery also works well when the temperature decreased to −20 °C as shown in Figure S5b (Supporting Information). Furthermore, the battery keeps its stable performance even after 150 cycles (Figure S5c, Supporting Information). The results correspond to the stable rate performance as shown in Figure 3a and Movie S3 (Supporting Information). The stable electrochemical performance of the lithium-ion cable battery may be attributed to strong interfacial bonding between active materials and CMF. The ultrahigh-tap density LTO-CMF electrode provides a capacity similar to that of LTO-Cu and exhibits the same electrochemical behavior. This phenomenon implies that the resistance of the "interface" between active materials and current collectors is also a critical parameter that is attributed to the performance of the battery. The internal resistance (IR) can be characterized by changes in voltage ($IR = IR_1 + IR_2$; Figure 3d) when charging (discharging) is switched to discharging (charging).[39] As shown in Figure 3d, at a rate of ≈2 C, LTO coated on CMF exhibited an IR change of ≈0.31 V, which is much lower than the corresponding value (0.76 V) for LTO coated on Cu foil. This result is also consistent at C-rates of up to 0.2–2 C (Figure S5d and Table S1, Supporting Information). In addition, the difference of IR changes is significant with the increase in C-rates. This suggests that despite the high electrical conductivity of Cu foil, CMF with its low interfacial resistance may be a good candidate for replacing metallic foils as current collectors in LIBs. Moreover, the flexibility of the batteries can be obtained. The insensitivity of the cable toward bending is also displayed in Figure S6 (Supporting Information). The voltage of the cable battery is very stable (maintained at 2.66 V all the time) even under harsh deformation conditions.

In the conventional design of the cable battery, the positive and negative tabs are arranged at each end of the cable to avoid short circuit as illustrated in previous reports.[18–34] In such design, the two tabs of the battery cannot be connected with electronics conventionally as the battery is woven or twisted randomly. In the present lithium-ion cable battery reported in this Communication, a flexible CMR was integrated in the battery system. The battery can be woven or twisted randomly and works well as both tabs of the battery could be integrated at the same side due to the use of the electrical conductivity of the CMR. The schematic diagram of the connection method is shown in **Figure 4**a. In Figure 4b, the lithium-ion cable battery can be twisted randomly. Furthermore, the luminescence of the lamps powered by the battery that is twisted around the arm showed no changes even after shaking for 30 min. The detailed process of shaking can be clearly seen in Movie S4 (Supporting Information). Moreover, the luminescence of the lamps did not change under the battery deformation, as shown in Movie S5 (Supporting Information).

The excellent flexibility of the lithium-ion cable battery is demonstrated in a linear guide system as shown in Figure 4c–j. The cable battery has been deformed. Guided by metal slide, the battery that fixes on the system could be deformed continuously. No differences were observed in discharge voltage profiles between deforming and no deforming conditions. It indicates that the lithium-ion cable battery can be successfully operated with an external strain. As shown in Figure 4c,d, the luminescence of the lamps powered by the battery experienced bending

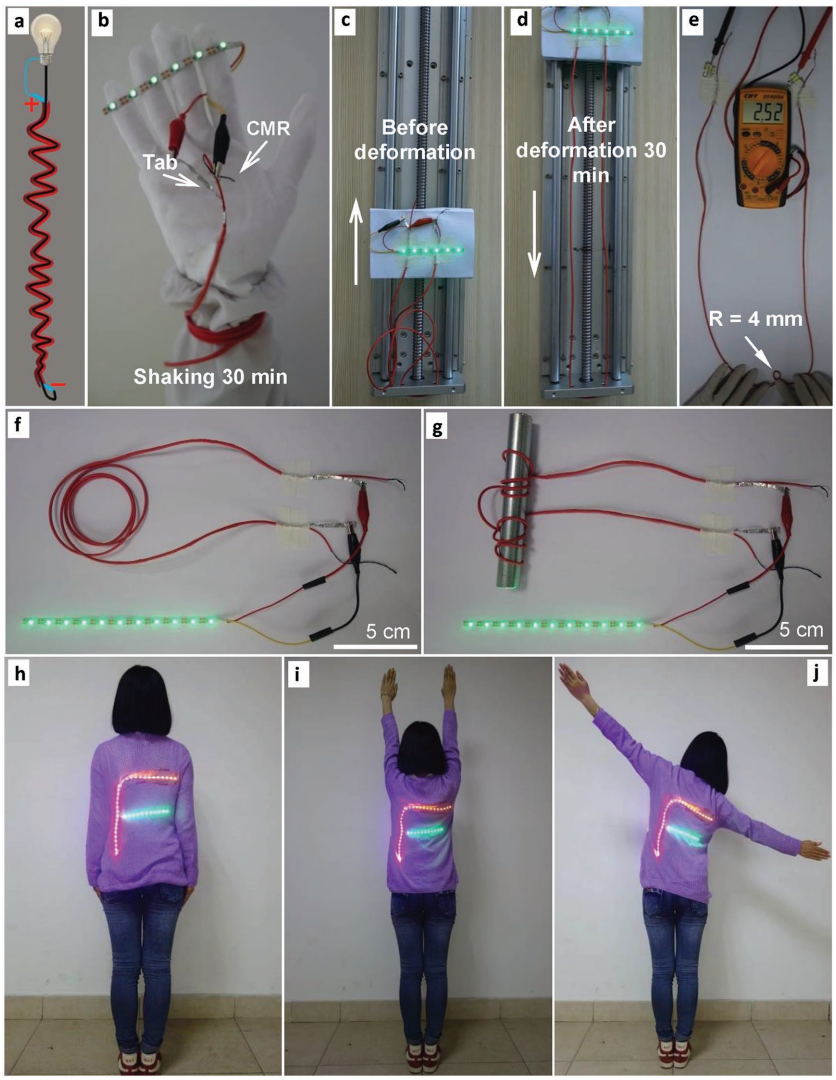

Figure 4. The demonstration of the operation, flexibility, and wearability of the lithium-ion cable battery. a) The schematic diagram and b) connection at the same side between battery; c,d) the LIB deforms in a linear guide system; e) the bending radius of the LIB at working state was measured; f) the battery at free state and g) twisted on a rod; and h–j) LED lights and the wearable lithium-ion cable battery on the body during exercises.

and stretching at 30 min does not have any change. The details of the deformation are shown in Movie S6 (Supporting Information). The results demonstrated that the performance of the flexible lithium-ion cable battery is unaffected by deformation. The extent of the deformation is determined by the bending radius of the cable battery. The bending radius of the battery at working state is shown in Figure 4e. The voltage measured by multimeter does not have any change after the battery was bent down to 4 mm. In addition, the voltage remained unchanged after cycling for 100 cycles. The bending radius could be further decreased because it is currently limited by the packaging material. The excellent electrochemical stability of the battery is clearly displayed in Movie S7 (Supporting Information). Conventional metal current collectors always show high density and poor flexibility, and impractical for weaving. All CNTs based on nonmetals used in the lithium-ion cable battery are more flexible and more applicable in wearable electronics with improved energy density. Under twisted deformations, the lamps connected with positive and negative tabs can still be powered. Moreover, the luminescence of the lamps does not have any obvious change even after the battery was subjected to four cycles of twisting and being released as shown in Figure 4f,g. The detailed process can be seen clearly in Movie S8 (Supporting Information).

The above results demonstrated that the new design of cable battery structure and the mechanical flexibility of the battery system are viable to their practical application for weaving. In addition, the performance of the woven battery is stable even under motion, as shown in Figure 4h,i and Movie S9 (Supporting Information). Therefore, the lithium-ion cable battery could be easily woven into textiles that allow breathing freely or can be integrated into materials that can fit the curved shape of the human bodies. High-specific capacity and energy density of the LIBs make them the first choice of energy storage for wearable electronics. The ultrahigh-specific capacity and ultrahigh-energy density should be obtained under ultrahigh-tap density of active materials on current collectors, representing a leap forward in energy storage capability of flexible energy storage devices. Recent achievements have developed specific capacity and energy density of the cable battery.[18–34] However, the results have not considered the tap density of the active materials on current collectors. In many cases, the tap density values were less than 2 mg cm^{-2}, which is much lower than commercial tap density for practical application.[40] In our study, the lithium-ion cable battery shows a volume specific capacity (calculated based on the total volume of the full battery) of 82.8 mAh cm^{-3}. This value is considerably higher than most of the previously reported cable-shaped batteries as shown in **Table 1** and Figure S7 (Supporting Information). Considering the open-circuit voltage and diameter of the cable, the volume energy density (volume-specific capacity × open-circuit voltage) of the flexible cable-shaped battery is ≈215 mWh cm^{-3}. The energy density of the battery is approximately seven times higher than that of the highest performance as previously reported, and this result is even impressively higher than that of sodium ion, zinc air, and other batteries with cable structures.[29–34]

Our findings demonstrated that lithium-ion cable battery based on CNTs favors to solve the most critical problems for flexible energy storage devices with strong mechanic flexibility, ultrahigh-energy density, and convenience of incorporation into the weaving process. The obtained battery displays excellent flexibility and stable electrochemical performances because of the use of flexible current collectors. In addition, the battery could be randomly wrapped around the body and be conventionally

Table 1. Comparison of the actual volume specific capacity, voltage, and actual volume energy density of the wearable lithium-ion cable battery based on CMF with other previous cable batteries.

Battery type	Voltage [V]	Specific capacity [mAh g^{-1}]	Active material mass loading [mg cm^{-2}]	Active material mass loading [mg cm^{-1}]	Battery diameter [mm]	Actual volume energy density [mWh cm^{-3}]
Titania/$LiMn_2O_4$ fiber battery[19]	3.5	168	Not provided	0.12–0.19	1.5	4.0–6.3
$LiMn_2O_4$-CNT/ $Li_4Ti_5O_{12}$-CNT[20]	2.5	138	0.01	0.02	1	0.89
$LiMn_2O_4$-CNTs/PI-CNTs[21]	1.4	120	0.002	0.01	2	0.05
$LiCoO_2$-Al/(Ni-Sn)-Cu[18]	1.7	1 mAh cm^{-1}	Not provided	1.3	2.5	20.4
Li-S[26]	2.1	600	0.05	0.2	1	32.1
Li-S[27]	2.1	343	2	2	3	20.4
Li-S[28]	2.1	335	0.28	0.04	2	0.9
Zinc-air[30]	0.9	Not rovided	0.796	2.4	10	3.6
Zinc-air[31]	1	12470	0.0014 n	0.05	3	5.7
Al-air[32]	1.65	935	0.07	0.01	3	0.22
Li/O_2-Ag -CNT[33]	2.0	500	0.005	0.008	5	0.04
Li/O_2-SP-carbon textiles-nickel foam [34]	2.0	500	0.5	0.5	10	0.64
This work	2.5–2.7	130	10	20	2	215

Note: Actual volume energy density = voltage × actual volume specific capacity.

connected to electronics after CMR was integrated due to the fact that both tabs can be led to the same end of the cable. Importantly, the active materials could be easily infiltrated into the porous surface of the current collectors, mitigating the delamination and increasing the tap density significantly up to 10 mg cm^{-2}, which leads to extremely high-energy density of 215 mWh cm^{-3}. The energy density of the cable battery is impressively higher (approximately seven times) than that of the highest performance as previously reported. This work provides a revolutionary way to enhance the energy density of the cable battery significantly. Such a CNT-based, novel-structured, and ultrahigh-energy density lithium-ion cable battery would solve some of the most critical problems for portable and flexible energy storage devices, indicating broad applications in wearable electronics.

Experimental Section

Preparation of CMFs and CMRs: The free standing CMFs were prepared through a methanol-mediated chemical vapor deposition at ≈1150 °C. Details of the preparation procedures can be found in our previous studies.[41,42] The CMR was prepared in the hot region of a reaction chamber by chemical vapor deposition method.[35,43] When CNTs were formed inside the chamber, CMR with a diameter of about 0.6 mm could be obtained by placing several strands of CNTs together and twisting them automatically with a speed of 100 r min^{-1} at both ends. The homogenous CMR could be obtained after passing through the drawing die (the size of the die hole is about 0.6 mm).

Coating Active Materials on CMFs: The electrodes were prepared using a slurry-based technique.[39] Super P carbon (SPC) (Timcal, Switzerland) was used as the conductive additive and polyvinylidene fluoride (PVDF, Arkema, France) was used as a binder. LTO (LTO-2, BTR) and LCO (YJGSL-5#, Beijing Easpring) were used as anode and cathode active materials, respectively. Anode slurry was prepared by LTO:SPC:PVDF at a weight ratio of 80:10:10, and cathode slurry was prepared by LCO:SPC:PVDF at a weight ratio of 90:4:6. *N*-methyl-2-pyrrolidone (Tianjin Damao) was used as the solvent for mixing. After that, the slurry was stirred for 8 h and then coated on the current collector and dried at 120 °C for 30 min. The tap density of the anode slurry after being dried on the CMF could be increased to a remarkably high mass loading of 10 mg cm^{-2} (the thickness of anode on CMF is about 65 µm after being rolled). To keep the same capacity for anode and cathode, the tap density of cathode slurry after being dried on the CMF should keep at 9.5 mg cm^{-2}; the thickness of cathode on CMF is about 55 µm after being rolled.

Assembling LIB-Integrated CMR: Polyethylene heat shrinkable tube was coated on CMR as the inner insulating layer; the diameter of the layer is about 1 mm after being shrunk. Then, the electrode of CMF-coated LCO on outer surface was wrapped around the insulating layer. Subsequently, the separator was wrapped around the cathode electrode. Then, anode on CMF was wrapped on the separator. The lithium-ion cable battery can be prepared after the polyethylene heat-shrinkable tube was sealed before electrolyte was injected into the cable in a dehumidification room at the moisture content of less than 5%; the diameter of the cable is about 2 mm after outside tube being shrunk. Polyethylene (2400, Celgard) film with thickness of about 12 µm was used as the separator. The solution of $LiPF_6$ (1 M) in diethyl carbonate and ethylene carbonate mixed at a weight ratio of 1:1 was used as electrolyte.

The Characterization of Electrodes and Batteries: The interface adhesion of LTO-CMF and LTO-Cu electrodes after being folded in half was observed by optical microscopy (Olympus DX51 microscope) and field emission SEM (FEI Sirion 200). The active materials were analyzed by XRD (D8 Advance, Bruker) using Cu Kα radiation. EIS measurements were performed on a CHI 760E electrochemical station. The performance of the obtained batteries was then measured by using Neware battery tester at room temperature. The galvanostatic charge/discharge was carried out in a potential window of 1.5–2.8 V. We state that we have obtained the informed signed consent from the volunteers in the work.

Supporting Information

Supporting Information is available from the Wiley Online Library or from the author.

Acknowledgements

This work was financially supported by the National Basic Research Program of China (Grant Nos. 2016YFA0200101 and 2014CB932500), the National Natural Science Foundation of China (Grant Nos. 51432002, 51520105003, 51362029, 51202095, and 51264010), the Department of Science & Technology of Jiangxi Province (Grant Nos. 20153BCB23011, GJJ150617, GJJ160596, and 20171ACB21043), and the program for Excellent Young Talents, JXUST. The authors also gratefully acknowledge the discussion with Prof. Nikhil Koratkar and Dr. Shravan Suresh at Rensselaer Polytechnic Institute.

Conflict of Interest

The authors declare no conflict of interest.

Keywords

cable-shaped, energy density, flexibility, wearable electronics

Received: January 30, 2018
Revised: March 16, 2018
Published online: April 23, 2018

[1] R. Mukherjee, A. Thomas, D. Datta, E. Singh, J. Li, O. Eksik, V. B. Shenoy, N. Koratkar, *Nat. Commun.* **2014**, *5*, 3710.
[2] Y. H. Zhu, Y. B. Yin, X. Yang, T. Sun, S. Wang, Y. S. Jiang, J. M. Yan, X. B. Zhang, *Angew. Chem., Int. Ed.* **2017**, *56*, 7881.
[3] Y. H. Zhu, X. Yang, D. Bao, X. B. Zhang, J. M. Yan, Q. Jiang, *Joule* **2018**, *2*, 1.
[4] H. G. Wang, W. Li, D. P. Liu, X. L. Feng, J. Wang, X. Y. Yang, X. B. Zhang, Y. J. Zhu, Y. Zhang, *Adv. Mater.* **2017**, *29*, 1703012.
[5] X. Y. Yang, J. J. Xu, D. Bao, Z. W. Chang, D. P. Liu, Y. Zhang, X. B. Zhang, *Adv. Mater.* **2017**, *29*, 1700378.
[6] F. L. Meng, H. X. Zhong, D. Bao, J. M. Yan, X. B. Zhang, *J. Am. Chem. Soc.* **2016**, *138*, 10226.
[7] L. Li, Z. Wu, S. Yuan, X. B. Zhang, *Energy Environ. Sci.* **2014**, *7*, 2101.
[8] L. B. Hu, H. Wu, F. L. Mantia, Y. Yang, Y. Cui, *ACS Nano* **2012**, *4*, 5843.
[9] Z. M. Song, T. Ma, R. Tang, Q. Cheng, X. Wang, D. Krishnaraju, R. Panat, C. K. Chan, H. Y. Yu, H. Q. Jiang, *Nat. Commun.* **2014**, *5*, 3140.
[10] L. Li, Z. P. Wu, H. Sun, D. M. Chen, J. Gao, S. Suresh, P. Chow, C. V. Singh, N. Koratkar, *ACS Nano* **2015**, *9*, 11342.
[11] J. W. Hu, Z. P. Wu, S. W. Zhong, W. B. Zhang, S. Suresh, A. Mehta, N. Koratkar, *Carbon* **2015**, *87*, 292.
[12] Q. C. Liu, T. Liu, D. P. Liu, Z. J. Li, X. B. Zhang, Y. Zhang, *Adv. Mater.* **2016**, *28*, 8413.
[13] L. Chen, G. M. Zhou, Z. B. Liu, X. M. Ma, J. Chen, Z. Y. Zhang, X. L. Ma, F. Li, H. M. Cheng, W. C. Ren, *Adv. Mater.* **2016**, *28*, 510.
[14] Q. H. Wang, S. W. Zhong, J. W. Hu, T. Liu, X. Y. Zhu, J. Chen, Y. Y. Hong, Z. P. Wu, *J. Power Sources* **2016**, *310*, 70.
[15] Y. X. Zeng, X. Y. Zhang, Y. Meng, M. H. Yu, J. N. Yi, Y. Q. Wu, X. H. Lu, Y. X. Tong, *Adv. Mater.* **2017**, *29*, 1700274.
[16] S. Y. Lee, K. H. Choi, W. S. Choi, Y. H. Kwon, H. R. Jung, H. C. Shin, J. Y. Kim, *Energy Environ. Sci.* **2013**, *6*, 2414.
[17] H. Sun, Y. Zhang, J. Zhang, X. M. Sun, H. S. Peng, *Nat. Rev. Mater.* **2017**, *2*, 17023.
[18] Y. H. Kwon, S. W. Woo, H. R. Jung, H. K. Yu, K. Kim, B. H. Oh, S. Ahn, S. Y. Lee, S. W. Song, J. Cho, H. C. Skin, J. Y. Kim, *Adv. Mater.* **2012**, *24*, 5192.
[19] T. Hoshide, Y. Zheng, J. Hou, Z. Wang, Q. Li, Z. Zhao, R. Ma, T. Sasaki, F. Geng, *Nano Lett.* **2017**, *17*, 3543.
[20] J. Ren, Y. Zhang, W. Y. Bai, X. L. Chen, Z. T. Zhang, X. Fang, W. Weng, Y. G. Wang, H. S. Peng, *Angew. Chem., Int. Ed.* **2014**, *53*, 7864.
[21] Y. Zhang, Y. H. Wang, L. Wang, C. M. Lo, Y. Zhao, Y. D. Jiao, G. F. Zheng, H. S. Peng, *J. Mater. Chem. A* **2016**, *4*, 9002.
[22] J. Ren, L. Li, C. Chen, X. L. Chen, Z. B. Cai, L. B. Qiu, Y. G. Wang, X. R. Zhu, H. S. Peng, *Adv. Mater.* **2013**, *25*, 1155.
[23] H. J. Lin, W. Weng, J. Ren, L. B. Qiu, Z. T. Zhang, P. N. Chen, X. L. Chen, J. Deng, Y. G. Wang, H. S. Peng, *Adv. Mater.* **2014**, *26*, 1217.
[24] W. Weng, Q. Sun, Y. Zhang, H. J. Lin, J. Ren, X. Lu, M. Wang, H. S. Peng, *Nano Lett.* **2014**, *14*, 3432.
[25] W. Weng, Q. Q. Wu, Q. Sun, X. Fang, G. Z. Guan, J. Ren, Y. Zhang, H. S. Peng, *J. Mater. Chem. A* **2015**, *3*, 10942.
[26] X. Fang, W. Weng, J. Ren, H. S. Peng, *Adv. Mater.* **2016**, *28*, 491.
[27] W. G. Chong, J. Q. Huang, Z. L. Xu, X. Y. Qin, X. Y. Wang, J. K. Kim, *Adv. Funct. Mater.* **2017**, *27*, 1604815.
[28] R. Q. Liu, Y. J. Liu, J. Chen, Q. Knag, L. L. Wang, W. X. Zhou, Z. D. Huang, X. J. Lin, Y. Li, P. Li, X. M. Feng, G. Wu, Y. W. Ma, W. Huang, *Nano Energy* **2017**, *33*, 325.
[29] Y. H. Zhu, S. Yuan, D. Bao, Y. B. Yin, H. X. Zhong, X. B. Zhang, J. M. Yan, Q. Jiang, *Adv. Mater.* **2017**, *29*, 1603719.
[30] J. Park, M. Park, G. Nam, J. S. Lee, J. Cho, *Adv. Mater.* **2015**, *27*, 1396.
[31] Y. F. Xu, Y. Zhang, Z. Y. Guo, J. Ren, Y. G. Wang, H. S. Peng, *Angew. Chem., Int. Ed.* **2015**, *54*, 15390.
[32] Y. F. Xu, Y. Zhao, J. Ren, Y. Zhang, H. S. Peng, *Angew. Chem., Int. Ed.* **2016**, *55*, 7979.
[33] Y. Zhang, L. Wang, Z. Y. Guo, Y. F. Xu, Y. G. Wang, H. S. Peng, *Angew. Chem., Int. Ed.* **2016**, *55*, 4487.
[34] T. Liu, Q. C. Liu, J. J. Xu, X. B. Zhang, *Small* **2016**, *12*, 3101.
[35] B. J. Han, T. Liu, Z. J. Huang, D. M. Chen, Y. S. Zhu, C. Y. Zhou, Y. S. Li, Y. H. Yin, Z. P. Wu, *Appl. Phys. Lett.* **2017**, *110*, 103902.
[36] P. L. Taberna, S. Mitra, P. Poizot, P. Simon, J. M. Tarascon, *Nat. Mater.* **2006**, *5*, 567.
[37] S. R. Gowda, A. L. M. Reddy, X. B. Zhan, H. R. Jafry, P. M. Ajayan, *Nano Lett.* **2012**, *12*, 1198.
[38] J. Xiao, W. Xu, D. Y. Wang, D. W. Choi, W. Wang, X. L. Li, G. L. Graff, J. Liu, J. G. Zhang, *J. Electrochem. Soc.* **2010**, *157*, A1047.
[39] K. Wang, S. Luo, Y. Wu, X. F. He, F. Zhao, J. P. Wang, K. L. Jiang, S. S. Fan, *Adv. Funct. Mater.* **2013**, *23*, 846.
[40] A. H. Whitehead, M. Schreiber, *J. Electrochem. Soc.* **2005**, *152*, A2105.
[41] Z. P. Wu, J. N. Wang, *Physica E* **2009**, *42*, 77.
[42] Z. P. Wu, M. M. Li, Y. Y. Hu, Y. S. Li, Z. X. Wang, Y. H. Yin, Y. S. Chen, X. Zhou, *Scr. Mater.* **2011**, *64*, 809.
[43] Z. P. Wu, W. B. Zhang, M. Zhao, Y. H. Yin, Y. Y. Hu, Y. S. Li, J. G. Yang, Q. F. Xu, *J. Appl. Phys.* **2014**, *115*, 124908.